Celestial Mech Dyn Astr (2007) 98:5–30
DOI 10.1007/s10569-007-9066-9

ORIGINAL ARTICLE

Dynamics of two satellites in the 2/1 Mean–Motion resonance: application to the case of Enceladus and Dione

N. Callegari Jr. · T. Yokoyama

Received: 29 August 2006 / Revised: 11 January 2007 /
Accepted: 13 January 2007 / Published online: 5 April 2007

Abstract The dynamics of a pair of satellites similar to Enceladus–Dione is investigated with a two-degrees-of-freedom model written in the domain of the planar general three-body problem. Using surfaces of section and spectral analysis methods, we study the phase space of the system in terms of several parameters, including the most recent data. A detailed study of the main possible regimes of motion is presented, and in particular we show that, besides the two separated resonances, the phase space is replete of secondary resonances.

Keywords Enceladus · Dione · Mean–Motion resonance · Periodic orbits · Regular and chaotic motion · Secondary resonance · Saturn

1 Introduction

The ratio of the mean motions of Enceladus and Dione around Saturn is approximately 1.993613, which is very near the ratio 2/1. Due to this commensurability, Enceladus–Dione system (hereafter denoted by E–D) is trapped in a libration such that their conjunctions occur on a line oscillating, around the pericenter of Enceladus, with period 11.5 years and small amplitude of the order of $1^0.4$ (Sinclair 1983). As the pericenters of the orbits of Enceladus and Dione circulate (mainly due to the high perturbation of Saturn oblateness), the previous conjunctions occur at any point of Dione orbit, circulating with period of about 3.8 years.

The role of the 2/1 commensurability in the dynamics of the pair E–D was investigated by several authors using analytical methods (Salgado and Sessin 1985; Bevilacqua and Sessin 1987; Bevilacqua et al. 1989; Message 1999), while others (Ferraz-Mello and Dvorak 1987; Karch and Dvorak 1988; Shinkin 2001) used numerical methods.

N. Callegari Jr. (✉) · T. Yokoyama
Departamento de Estatística, Matemática Aplicada e Computação,
UNESP, Rio Claro, SP, Brasil
e-mail: calleg@rc.unesp.br

In this work we revisit the same problem, taking a semi-analytical method, where the whole dynamics is studied in the framework of the general three-body planar problem. We have included the oblateness of the planet through J_2 and J_4 terms, the main critical angles associated to the 2/1 resonance up to power two in the eccentricities (i.e., the two critical angles associated to the resonances of Enceladus and Dione and their first harmonics), and the secular and long-period terms of the disturbing function. Tittemore and Wisdom (1988, 1990) have shown that a similar model has two degrees of freedom, and therefore its dynamics can be studied with the technique of surfaces of section. Here we also use this technique, and the results are checked and complemented with the spectral dynamical map method developed by (Michtchenko and Ferraz-Mello 2001). The aim of this work is to obtain a detailed study of the phase space of the 2/1 Mean–Motion resonance in E–D system.

The current configuration of the E–D pair was probably reached by tidal evolution (Goldreich 1965; Sinclair 1972, 1983; Henrard and Lemaitre 1983; Peale 1986, 1999, 2003). It is also believed that the observed resurfacing of Enceladus crust might be related to the resonant dynamics of the system (Peale 2003; Spencer et al. 2006). In this work we will limit ourselves to the conservative dynamics.

We have organized this paper in the following way: the model, some steps in its derivation, and the set of the parameters used are discussed in Sect. 2. In Sect. 3, we show several sets of initial conditions of the pair E–D in different parametric configurations. In Sect. 4, the core of this paper, the phase space of the system in a representative plane of initial conditions, is studied in high detail through surfaces of section and spectral analyses. The conclusions are given in Sect. 5.

2 Model and initial parameters

Let us begin writing the Hamiltonian of a system formed by N satellites with masses m_i, orbiting a parent planet with mass M. A canonical set of variables introduced by Poincaré (Hori 1985; Laskar and Robutel 1995; Ferraz-Mello et al. 2006) allows us to write the Hamiltonian for the general form of $N+1$ body problem. Let $\vec{r_i}$ be the position vectors of the satellites relative to the center of the planet, and $\vec{p_i}$ be the momentum vectors relative to the center of mass of the system. The pair $(\vec{r_i}, \vec{p_i})$ form a canonical set of variables with the Hamiltonian given by

$$H = H_0 + H_1 + H_J \tag{1}$$

where:

$$H_0 = \sum_{i=1}^{N} \left(\frac{|\vec{p_i}|^2}{2\beta_i} - \frac{\mu_i \beta_i}{|\vec{r}_i|} \right), \tag{2}$$

$$H_1 = -G \sum_{0<i<j} \left(\frac{m_i m_j}{\Delta_{ij}} + \frac{\vec{p_i} \cdot \vec{p_j}}{M} \right), \quad j = 1, \ldots, N, \tag{3}$$

$$H_J = -\sum_{i=1}^{N} \frac{\mu_i \beta_i}{|\vec{r}_i|} \left[-\sum_{l=2}^{\infty} J_l \left(\frac{R_e}{|\vec{r}_i|} \right)^l P_l(\sin \varphi_i) \right], \tag{4}$$

where $\mu_i = G(M + m_i)$, $\beta_i = \frac{Mm_i}{M+m_i}$, $\Delta_{ij} = |\vec{r_i} - \vec{r_j}|$, G is the gravitational constant. $\jmath_l$ are the zonal oblateness coefficients; $l = 2$ or 4 as mentioned below; $P_l(\sin\varphi_i)$ are the classical Legendre polynomials and φ_i are the latitudes of the satellites referred to the equator of the planet. The chosen units are: the equatorial radius of the planet (R_e), day and mass of the planet. Equation (2) defines the Keplerian motion of each satellite around the planet, while Eq. (3) gives the mutual interaction among the satellites and Eq. (4) represents the perturbation of the non-sphericity of the planet. In Eq. (1) we take $N = 2$, and in Eq. (4) we take $l = 2$ and 4.

2.1 The planar model

In order to obtain a simplified version of the Hamiltonian (1) for the case of E–D, we make several expansions and simplifications. Our model is an extension of the previous one given in Callegari et al. (2004), developed for the "planetary case". The main difference between a planetary and regular satellite system is the perturbation of the oblateness of the central body.

The expansion of the right-hand side of the Eqs. (2), (3) and (4) are resumed as follows. In the case of H_0, we first use the Hamilton–Jacobi theory to rewrite it in the form

$$H_0 = -\sum_{i=1}^{2} \frac{\mu_i \beta_i}{2a_i}, \tag{5}$$

where a_i is the semi-major axis of each satellite orbit.

The expanded form of Eq. (3) can be obtained from classical expressions of the disturbing function. Keeping only the main resonant and secular terms in the expression of the disturbing function, considering only the planar case since the orbital inclinations of Enceladus and Dione relative to Saturnian equator are negligible (Peale 1999), we have,

$$H_1 = H_{\text{sec}} + H_{\text{res}}, \tag{6}$$

where

$$H_{\text{sec}} = -\frac{Gm_1m_2}{a_2}\left[a + b\left(\frac{e_1^2}{2} + \frac{e_2^2}{2}\right) + c\left(\frac{e_1}{2}\right)\left(\frac{e_2}{2}\right)\cos(\varpi_1 - \varpi_2)\right], \tag{7}$$

$$\begin{aligned} H_{\text{res}} = -\frac{Gm_1m_2}{a_2} \times \Bigg\{ & d\left(\frac{e_1}{2}\right)\cos\left[(1+r)\lambda_2 - r\lambda_1 - \varpi_1\right] \\ & + e\left(\frac{e_2}{2}\right)\cos\left[(1+r)\lambda_2 - r\lambda_1 - \varpi_2\right] \\ & + g\left(\frac{e_2^2}{2}\right)\cos 2\left[(1+r)\lambda_2 - r\lambda_1 - \varpi_2\right] \\ & + f\left(\frac{e_1^2}{2}\right)\cos 2\left[(1+r)\lambda_2 - r\lambda_1 - \varpi_1\right] \\ & + h\left(\frac{e_1}{2}\right)\left(\frac{e_2}{2}\right)\cos 2\left[(1+r)\lambda_2 - r\lambda_1 - \frac{1}{2}\varpi_1 - \frac{1}{2}\varpi_2\right]\Bigg\}, \end{aligned} \tag{8}$$

where e_i, λ_i, ϖ_i are the eccentricity, mean longitude and longitude of pericenter of the satellites, respectively; the coefficients a–h are functions of the ratio $\alpha = a_1/a_2$ and $r = p/q$, where $p = q = 1$ for the 2/1 resonance (Callegari et al. 2004).

The secular part of the oblateness perturbation given in Eq. (4) is

$$H_{\mathrm{J}}|_{aver.} = \sum_{i=1}^{2} \left(1 - e_i^2\right)^{-\frac{3}{2}} \left[-\frac{\mu_i \beta_i \mathrm{J}_2 R_e^2}{2a_i^3} + \frac{\mu_i \beta_i \mathrm{J}_4 R_e^4}{8a_i^5} \left(1 + \frac{3}{2} e_i^2\right) \right]. \tag{9}$$

Let us define the following set of canonical variables

$$\begin{array}{ll} I_1 = L_1 - G_1, & \sigma_1 = (1+r)\lambda_2 - r\lambda_1 - \varpi_1; \\ I_2 = L_2 - G_2, & \sigma_2 = (1+r)\lambda_2 - r\lambda_1 - \varpi_2; \\ \Gamma_1 = L_1 + r(I_1 + I_2), & \lambda_1; \\ \Gamma_2 = L_2 - (r+1)(I_1 + I_2), & \lambda_2, \end{array} \tag{10}$$

where $L_i = \beta_i \sqrt{\mu_i a_i}$, $G_i = L_i \sqrt{1 - e_i^2}$. Expanding Eqs. (5), (6) and (9) in power of I_i, $i = 1, 2$ up to first order we obtain:

$$\begin{aligned} H = {} & H_{\mathrm{const.}} + 2A(I_1 + I_2) + 4B(I_1 + I_2)^2 \\ & + 2CI_1 + 2DI_2 + 2E\sqrt{I_1 I_2}\cos(\sigma_1 - \sigma_2) \\ & + F\sqrt{2I_1}\cos\sigma_1 + I\sqrt{2I_2}\cos\sigma_2 + 2K\sqrt{I_1 I_2}\cos(\sigma_1 + \sigma_2) \\ & + 2RI_1\cos 2\sigma_1 + 2SI_2\cos 2\sigma_2 \end{aligned} \tag{11}$$

where $H_{\mathrm{const.}} < 0$ is the constant part of Hamiltonian, which will be neglected in all calculations in this paper, and $A-F, I, K, R, S$ are constant coefficients. Table 2 gives the expression of the coefficients and their numerical values, which were calculated with the parameters adopted in Table 1. In Table 2, the two quantities, Γ_1 and Γ_2, are integrals of the motion, since in the averaged Hamiltonian written in terms of variables defined in (10), the coordinates λ_1, λ_2 are cyclic. The model has therefore two degrees of freedom.

In (11), the terms with coefficients A and B come from the Keplerian part (5), and those with coefficients C, D and E are due to the secular (7) and Keplerian part. Terms factored by F and I define the main resonance (Enceladus and Dione resonances, respectively), and those with coefficients K, R, S are the corresponding second harmonics. Sometimes (e.g., Peale 1986) the importance of the combination of $(\sigma_1 + \sigma_2)$ is considered at the same level of the terms $F\sqrt{2I_1}\cos\sigma_1$ and $I\sqrt{2I_2}\cos\sigma_2$. However since $(\sigma_1 + \sigma_2)$ only appears with the factor $2K\sqrt{I_1 I_2}$, we prefer to define as main resonances only the terms $F\sqrt{2I_1}\cos\sigma_1$ and $I\sqrt{2I_2}\cos\sigma_2$.

Table 1 Set of parameters used in the calculation of the coefficients given in Table 2

	(1) J_2 ($\times 10^6$)	(2) J_4 ($\times 10^6$)	(3) M ($M_\odot$)	(4) R_e (km)
Saturn	16291.8579	−931.1922	1/3499.29	60268
	(5) Mass ($M \times 10^{-7}$)	(6) Semi-major axes (R_e)	(7) Period (day)	(8) Eccentricity
Enceladus	1.5217	3.9558382	1.374612	0.0045
Dione	19.2794	6.2661284	2.740444	0.0022

1–2: Jacobson (2004); 3–8: Collected from http://ssd.jpl.nasa.gov/horizons.html in 2005, where the values of the semi-major axes are given for 2005-Jan-01 00:00

Table 2 Expressions of the coefficients of the Hamiltonian (12) and integrals Γ_i and their numerical values

Coefficient	Numerical value
$A = \frac{1}{2}GM\left[-\frac{k_1 r}{\Gamma_1^3} + \frac{k_2(r+1)}{\Gamma_2^3}\right]$	7.6983×10^{-3}
$B = -\frac{3}{8}GM\left[\frac{k_1 r^2}{\Gamma_1^4} + \frac{k_2(r+1)^2}{\Gamma_2^4}\right]$	-177261.1194
$C = \frac{1}{2}k_{12}\left\{\frac{-b}{\Gamma_1\Gamma_2^2} + \frac{2(r+1)a}{\Gamma_2^3} + \frac{2}{\Gamma_2^2}\frac{da}{d\alpha}\frac{\beta_2^2\mu_2}{\beta_1^2\mu_1}\left[\frac{\Gamma_1 r}{\Gamma_2^2} + \frac{\Gamma_1^2(r+1)}{\Gamma_2^3}\right]\right\}$ $+T_{j2c} + T_{j4c}$	-7.897728×10^{-3}
$D = \frac{1}{2}k_{12}\left\{\frac{1}{\Gamma_2^3}\left[-b + 2(r+1)a\right] + \frac{2}{\Gamma_2^2}\frac{da}{d\alpha}\frac{\beta_2^2\mu_2}{\beta_1^2\mu_1}\left[\frac{\Gamma_1 r}{\Gamma_2^2} + \frac{\Gamma_1^2(r+1)}{\Gamma_2^3}\right]\right\}$ $+T_{j2d} + T_{j4d}$	-5.021339×10^{-3}
$E = -\frac{k_{12}c}{4\Gamma_2^2\sqrt{\Gamma_1\Gamma_2}}$	8.113136×10^{-7}
$F = -\frac{k_{12}d}{2\Gamma_2^2\sqrt{\Gamma_1}}$	2.198007×10^{-8}
$I = -\frac{k_{12}e}{2\Gamma_2^2\sqrt{\Gamma_2}}$	-4.897480×10^{-9}
$K = -\frac{k_{12}h}{4\Gamma_2^2\sqrt{\Gamma_1\Gamma_2}}$	6.9785637×10^{-6}
$R = -\frac{k_{12}f}{8\Gamma_1\Gamma_2^2}$	$-5.3880293 \times 10^{-6}$
$S = -\frac{k_{12}g}{8\Gamma_2^3}$	$-1.2618983 \times 10^{-6}$
Γ_1	1.088523×10^{-5}
Γ_2	1.735596×10^{-4}

where $r = p = 1$ and,

$$
\begin{aligned}
&k_1 = \mu_1\beta_1^2 m_1, k_2 = \mu_2\beta_2^2 m_2, k_{12} = Gm_1m_2\mu_2\beta_2^2;\\
&T_{j2c} = 1.5(1+2p)C_1 - 3(1+p)C_2, \quad T_{j4c} = (3+5p)C_3 - 5(1+p)C_4,\\
&T_{j2d} = 3pC_1 - 1.5(1+2p)C_2, \quad T_{j4d} = 5pC_3 - 5(2+5p)C_4;\\
&C_1 = \frac{c_{11}\beta_1^6\mu_1^3}{\Gamma_1^7}, \quad C_2 = \frac{c_{12}\beta_2^6\mu_2^3}{\Gamma_2^7}, \quad C_3 = \frac{c_{21}\beta_1^{10}\mu_1^5}{\Gamma_1^{11}}, \quad C_4 = \frac{c_{22}\beta_2^{10}\mu_1^5}{\Gamma_2^{11}};\\
&c_{11} = -\frac{1}{2}GMm_1R_e^2\mathrm{J}_2, \quad c_{12} = -\frac{1}{2}GMm_2R_e^2\mathrm{J}_2,\\
&c_{21} = +\frac{3}{8}GMm_1R_e^4\mathrm{J}_4, \quad c_{22} = +\frac{3}{8}GMm_2R_e^4\mathrm{J}_4
\end{aligned}
$$

In terms of the non-singular Poincaré variables $x_i = \sqrt{2I_i}\cos\sigma_i$, $y_i = \sqrt{2I_i}\sin\sigma_i$, the Hamiltonian is given by

$$
\begin{aligned}
H = {} & A(x_1^2 + y_1^2 + x_2^2 + y_2^2) + B(x_1^2 + y_1^2 + x_2^2 + y_2^2)^2\\
& + C(x_1^2 + y_1^2) + D(x_2^2 + y_2^2) + E(x_1x_2 + y_1y_2)\\
& + Fx_1 + Ix_2\\
& + K(x_1x_2 - y_1y_2) + R(x_1^2 - y_1^2) + S(x_2^2 - y_2^2).
\end{aligned} \tag{12}
$$

2.2 The current status of the system

It is well known (Sinclair 1972; Henrard and Lemaitre 1983) that σ_1 oscillates around zero with small amplitude and very small free eccentricity ($\sim 10^{-4}$), due to the

existence of a non zero (~ 0.0045) value of forced eccentricity of the Enceladus orbit caused by the proximity of the 2/1 resonance. Similar kind of motion where the critical angle librates, without the existence of a separatrix isolating the circulation from the libration regime will be denoted here by paradoxical libration (e.g., Sessin and Ferraz-Mello 1984; Ferraz-Mello 1985). In order to check our model, let us do some trivial tests with averaged equations of motion, with the aim to see whether Hamiltonian (12) is appropriate to recover qualitatively the current status of E–D.

We have integrated numerically the four Hamilton equations associated to Eq. (12)[1]. We consider initial condition where σ_1 is near zero and σ_2 is arbitrary because it is circulating. Figure 1 shows two examples with σ_1 librating in the averaged system around zero with period around 11.5 years, and σ_2 circulating in direct direction with period of about 3.5 years, similar to the current configuration of the pair E–D (Sinclair 1972). From numerical experiments we conclude that the period of σ_i and forced eccentricities are not so sensitive to slight changes in the initial conditions. However the libration of σ_1 is quite sensitive for different choices of the semi-major axes.

To close this section, we mention that our constants and parameters are defined according to Tables 1 and 2 and despite of some uncertainty or sensitivity in the input data, our averaged model is complete enough to recover and explore the global qualitative dynamics of the problem.

3 Representative planes of initial conditions

Having in mind that we are going to use surfaces of section, it is very useful to exhibit some features and location of the initial conditions we are going to select. To this end, we define a plane of initial conditions, which we call representative plane. Since in the surfaces of section method, the energy is the common parameter for any orbit, let us draw some equi-energy curves in a plane. The initial conditions will be taken choosing some curves in this plane.

We define our representative plane in the following way: from Hamiltonian (12) we fix $\sigma_i = 0$ or π, $i = 1, 2$. Then H becomes a function of e_1 and e_2 only, so that equi-H curves are easily obtained solving numerically $H(e_1, e_2) = const.$. Unfortunately fixing $\sigma_i = 0$ or π means that some asymmetric stable configurations (Jancart et al. 2002; Beaugé et al. 2005) cannot be covered in our study. Even so, our (e_1, e_2) representative plane will give a large variety of interesting regions. The more complex the structures of the curves in this plane, the more regimes of motion are expected.

The representative plane can be obtained by plotting the contours of the function $H = f(e_1, e_2)$, as depicted in Fig. 2. From (12), we can show that, for low eccentricities, $H = f(e_1, e_2)$ is a quartic polynomial with respect to e_1 and e_2. For instance, considering the level curve l_1 ($H = -6.25 \times 10^{-12}$) in Fig. 2, the four open circles r_1, r_2, r_3 and r_4 on the energy level are four values of e_2 corresponding to $e_1 = -0.021$. In fact, in most cases, there may exist up to four real roots (e_2) of the eccentricity of the outer satellite. The roots r_1 and r_2 correspond, in general, to $\sigma_2 = \pi$ ($e_2 < 0$) while roots r_3 and r_4 correspond, in general, to $\sigma_2 = 0$ ($e_2 > 0$). The pairs (r_2,r_3) and (r_1,r_4) will be called inner and outer pair, respectively.

[1] The mean elements obtained are given in Poincaré system, and therefore are not osculating—Ferraz-Mello et al. 2006.

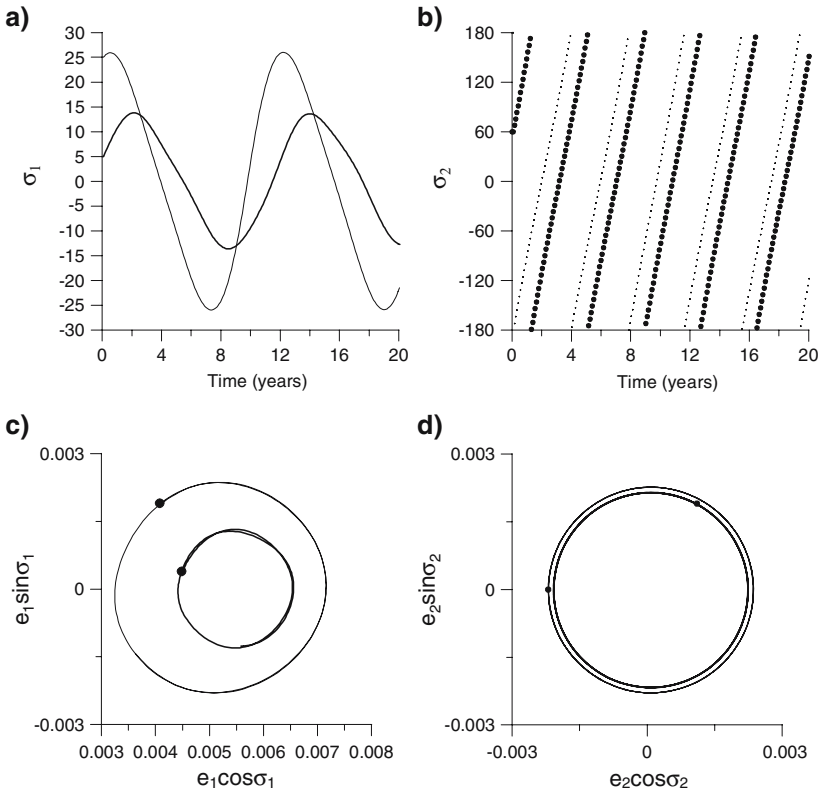

Fig. 1 (**a, b**) Time evolution of the critical angles σ_1 and σ_2 for two sets of initial conditions: $\sigma_1 = 5^0$, $\sigma_2 = 60^0$ (bold lines), and $\sigma_1 = 25^0$, $\sigma_2 = 180^0$ (thin lines); in both cases, $e_1 = 0.0045$, $e_2 = 0.0022$. (**c, d**) The same plots as shown in (**a, b**) in the variables $e_i \cos\sigma_i \times e_i \sin\sigma_i$. The black points indicate initial conditions

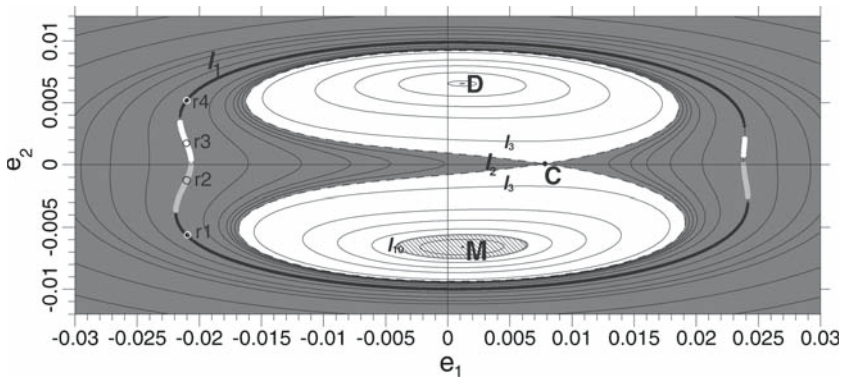

Fig. 2 Representative plane of initial conditions. Each curve is a level curve of the Hamiltonian (12), adopting σ_1 and σ_2 fixed at zero or π. Positive and negative e_1 and e_2 correspond to $\sigma_i = 0$ and $\sigma_i = \pi$, respectively. All symbols given by open circles r_1-r_4, points C, D, M, and three distinct region given in gray, white and hatched are discussed in Sect. 3. The numerical values of typical level curves (as l_1, l_2, l_3, l_{10}) are given in Table 4

For each energy value, the four real roots are distributed in four families of initial conditions, which will be also called here r_1, r_2, r_3 and r_4. For instance, in the case of level curve l_1 in Fig. 2, the outer families r_1 and r_4 are given by bold lines, the inner family r_2 is given in gray, and the r_3 inner family is indicated by white lines. Note that any orbit of our problem belongs to one level curve with fixed energy and besides this, it also falls in one and only one subset of solutions which we have called families r_1, r_2, r_3 and r_4. To group the solutions in these families is very important as we will see in Sect. 4.

Figure 2 shows several contour curves which are distributed on the representative plane in three main regions, which are delimited by the curves passing through the zero-gradient points, C, D and M. The level curves with energies smaller than the corresponding value of l_2, plotted with dashed line in Fig. 2, belong to gray region, and will be studied in Sect. 4.1. For level curves with energy larger than l_2 and smaller than l_{10}, given in gray-bold line, we are in the white portion of Fig. 2 where the representative plane is divided in two parts, sharing the common point C. The dynamics in this region will be studied in Sects. 4.2–4.4. A third region (hatched region) is delimited by the energy levels l_{10} and M (the point near the maximum value of energy, where $H \approx 10.5745 \times 10^{-12}$), will be the last region to be studied. For $e_2 > 0$ the level curve l_{10} shrinks and becomes a point, which is labeled by D in Fig. 2. In other words, this shows clearly that Fig. 2 is not symmetric. On the other hand, almost all solutions of the hatched region belong to family r_1 or r_2.

As discussed in Sect. 2.2, the dynamics of the pair E–D is sensitive to the initial parameters. In order to investigate how the shapes of the energy levels of the Hamiltonian (12) depend on these parameters, we plot some level curves for different values of semi-major axes and Enceladus mass, which are the three most uncertain "dynamical" parameters of the system.

In the case of semi-major axes of Enceladus and Dione, instead of taking arbitrary values of these quantities around the current one, let us calculate some probable values of them which might have been attained during a possible tidal evolution of the system. For this task we use the simplified expression of the semi-major axes variation due to tides on Saturn (e.g., Peale 1999):

$$a_i^{13/2} = a_{0i}^{13/2} + c(t - t_0), \quad c = \frac{39 k_2 \sqrt{G/M} R_e^5 m_i}{2 Q_S}, \tag{13}$$

where $t_0 = 4.5 \times 10^9$ years is the stipulated age of the Solar system, t is the past time, a_{0i} are the current semi-major axes (Table 1), $k_2 = 0.34$ is a value adopted for the k-Love number of Saturn and $Q_S = 14000$ is a minimum plausible value of the dissipation function of Saturn (Peale 2003).

Different choices of the semi-major axes correspond to distinct values of the coefficients of the Hamiltonian (12) (Table 3). Among all coefficients, Table 3 may be used to show that A is the most sensitive to changes in the semi-major axes. In fact, for near circular orbits, the expression for the coefficient A is well approximated by $A \sim \frac{1}{2}[2n_2 - n_1]$, where n_1, n_2 are the mean motions. Therefore, it is enough to redraw Fig. 2 with different values of A, what is shown in Fig. 3(a–c).

Figure 3(a) corresponds to $A = 0.000379$ ($\alpha = 0.629960$), which is very close to the exact 2/1 commensurability, but the topology of the level curves is very different from Fig. 2. Just at a glance we can see that the eight-shaped curve appears when the adopted ratio of the semi-major axes is $\alpha = 0.630867$, slightly smaller than the value

Table 3 Numerical values of some parameters and coefficients of the Hamiltonian used in Fig. 3

Figure	parameter	Coefficients
3(a)	$a_1 = 3.932925, a_2 = 6.243134$ ($\alpha = 0.629960$)	$A = 0.000379$, $B = -179247.2303$ $C = -8.082183 \times 10^{-3}$, $D = -5.141162 \times 10^{-3}$, $F = 2.196291 \times 10^{-8}$, $I = -4.88714 \times 10^{-9}$
3(b)	$a_1 = 3.949003, a_2 = 6.259241$ ($\alpha = 0.630908$)	$A = 0.005548$
3(c)	$a_1 = 3.960100, a_2 = 6.270400$ ($\alpha = 0.631555$)	$A = 0.009044$
3(d)	$m_1 = 2.61 \times 10^{-7}$	$A = 0.00759$
3(e)	$m_1 = 0.19 \times 10^{-7}$	$A = 0.00954$
3(f)	$m_1 = 1.9007 \times 10^{-7}$, $m_2 = 19.2752 \times 10^{-7}$, $J_2 = 16290.6/10^6, J_4 = -936.0/10^6$, $M = 1/3499.928\ M_\odot$ (Jacobson et al. 2005)	$A = 0.0076470$, $B = -145879.8111$, $C = -7.896963 \times 10^{-3}$, $D = -5.020840 \times 10^{-3}$, $F = 2.455613 \times 10^{-8}$, $I = -6.115516 \times 10^{-9}$

Units are the same as in Table 1. The column 2 lists the parameters that have changed, and all the remaining parameters are the same of Table 1

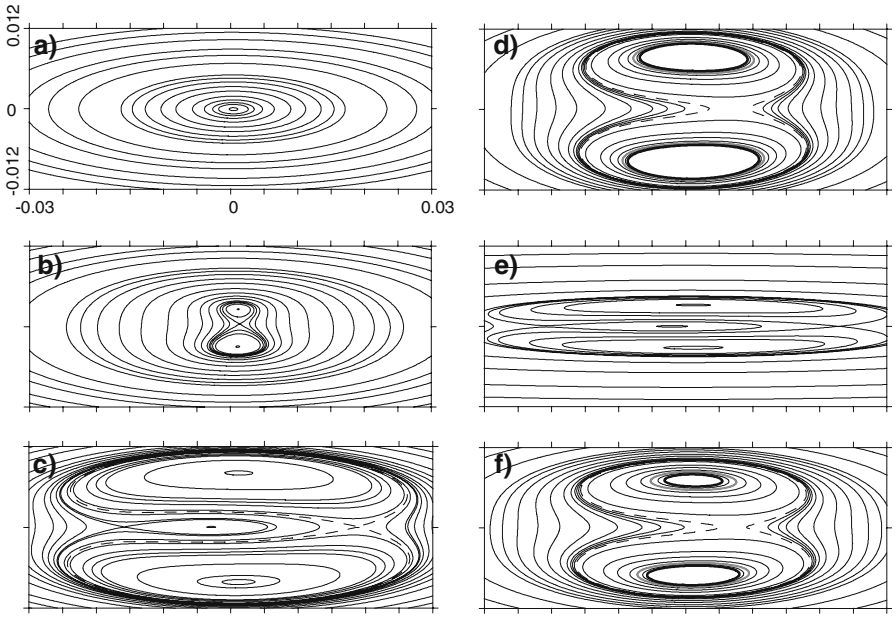

Fig. 3 (**a–c**) The same as Fig. 2, for different values of semi-major axes of the pair E–D. (**d, e**) The same as (**a–c**), for different values of Enceladus mass. (**f**) The same as (**a–c**) for the current set of masses and oblateness coefficients. The numerical values of the parameters utilized here are given in Table 3. The scales in all figures are the same as (**a**). In (**d**) and (**f**), the set energy levels are the same as utilized in Fig. 2

of α given in Fig. 3(b). For these values of the semi-major axes we can reproduce Fig. 2, which geometry is characterized by the presence of the three critical points C, D and M. For values of semi-major axes larger than the "current" ones adopted in Table 1, a new bifurcation appears near the center of the figure, as is shown in Fig. 3(c).

Figure 3(a–c) show that the general behavior of the level curves is very sensitive to the adopted values of a_1 and a_2. Moreover, small changes in α may cause the appearance/disappearance of different regions as shown in Fig. 2. It is worth to notice the following points: as briefly discussed in Sect. 2.2, the dynamics of the dynamical system (12) depends on the choice of the adopted parameters. Now we see that this choice in fact defines the representative plane. In this work we have adopted Fig. 2 for several reasons. First, the adopted set of parameters allows us to reproduce qualitatively the dynamical properties of the "current" system. Second, the representative plane given by Fig. 2 is sufficiently complex to reveal almost all the important characteristics of the phase space, which are given by the two main resonances of Enceladus and Dione, and the most important secondary resonances, as we will see in Sect. 4. Third, values of the semi-major axes of Enceladus and Dione slightly smaller or larger than the "current" values listed in Table 1, lead to representative planes similar to Fig. 2 (see Fig. 3b). Quite complex cases occur for sets of the semi-major axes very larger than the "current" one (as shown in Fig. 3c). The same occurs for very distinct values of some parameters, for instance, the Enceladus mass (see below). However, the dynamics of these complex scenarios shown in Fig. 3 will not be studied in this paper, since this subject will be undertaken in a future paper.

The dependence of the level curves with respect to the mass of Enceladus is shown in Fig. 3(d, e). In Fig. 3(d) we consider the largest value of Enceladus mass that we found in the literature: $m_1 = 2.61 \times 10^{-7}\, M$ (see Jacobson et al. 2006, and references therein). We see that the structure of the level curves observed in Fig. 2 is maintained, and the main change is given by a higher deformation of the level curves in e_2 axis, which is expected since the higher is m_1, the stronger will be the perturbation of Enceladus on Dione orbit. The opposite occurs using the smallest value of m_1 given by $m_1 = 0.19 \times 10^{-7}\, M$, as we show in Fig. 3(e): in this case, a new center near the origin of the figure arises (similar to Fig. 3c), changing significantly the topology.

Recently, due to Cassini mission, more precise data of Saturnian system were issued (Table 3; Jacobson et al. 2005). Figure 3(f) is obtained with these new data, but there is almost no difference when compared to Fig. 2.

4 Dynamics of the 2/1 mean–motion resonance

As our dynamical system has two degrees of freedom, the surfaces of section technique can be used in the study of the dynamics. We can define two surfaces of section (Tittemore and Wisdom 1988): one related to the inner satellite motion (here called Enceladus section), and another one for the outer satellite (Dione section). The Enceladus section is defined through the condition $y_2 = 0$ and is represented on the plane $(e_1 \cos\sigma_1 \times e_1 \sin\sigma_1)$. The Dione section is defined through the condition $y_1 = 0$ and is represented on the plane $(e_2 \cos\sigma_2 \times e_2 \sin\sigma_2)$. The above conditions of the sections $(y_i = 0)$ are done according to the initial direction of the flux, which depends on the set of initial conditions. In the case of the inner family r_1, we take $\frac{\mathrm{d}y_2}{\mathrm{d}t}|_0 > 0$

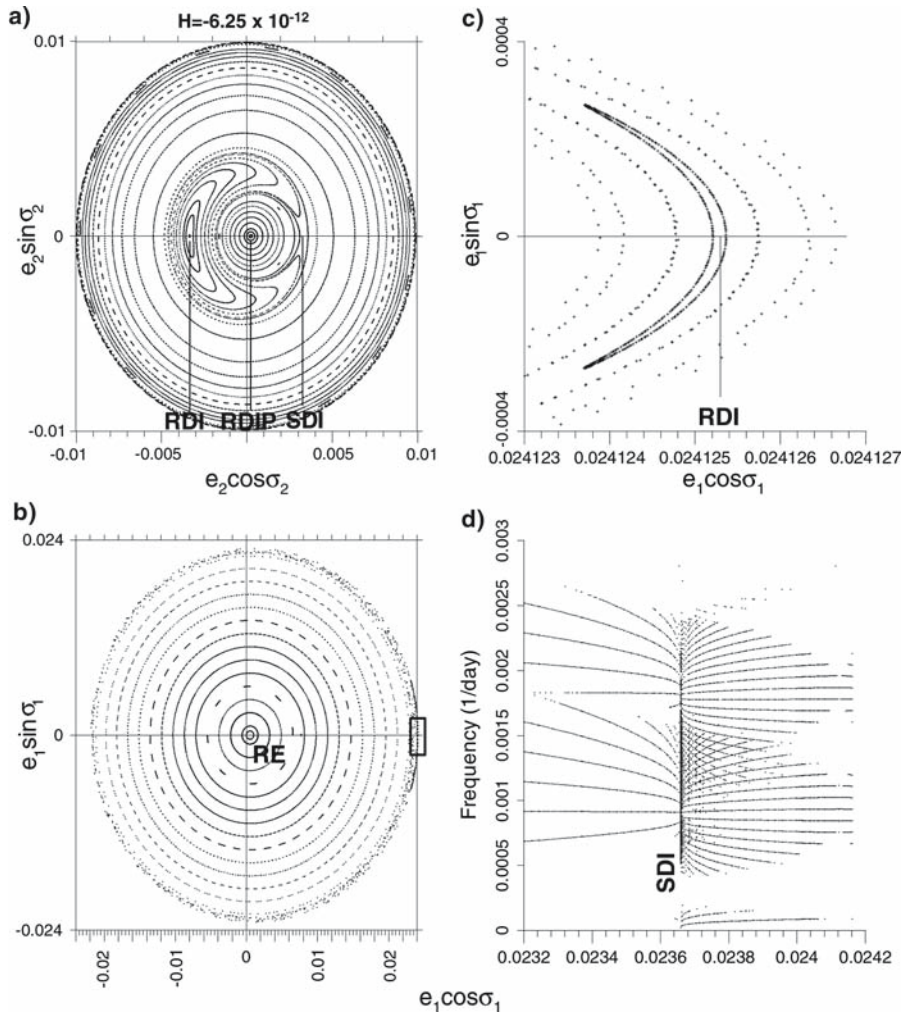

Fig. 4 (**a**) Surfaces of section of Dione (Dione section). The value of energy is indicated at the top, and the main regimes of motion at the bottom of the figure. (**b**) Surfaces of section of Enceladus (Enceladus section). (**c**) Detail around the center RDI in the region of Enceladus section drawn in black rectangle in (**b**). (**d**) IPS corresponding to a portion in Enceladus section around SDI

in the Enceladus section, and $\frac{dy_1}{dt}|_0 < 0$ in the Dione section. In the case of the inner family r_2, we consider $\frac{dy_2}{dt}|_0 < 0$ in the Enceladus section, and $\frac{dy_1}{dt}|_0 < 0$ in the Dione sections.

In this work, all surfaces of sections are done with the family r_2, except in Fig. 4 and in the Appendix, where we use the family r_1. The reason will be clear in Sect. 4.3: the family r_2 passes through the region of phase space where all important periodic orbits are present. If we have preferred to choose the family r_1, for instance, several important aspects of the dynamics would be lost (Callegari et al. 2004, 2006).

We also construct individual dynamic power spectra (hereafter denoted by IPS), for the set of solutions with initial condition $e_1 \sin\sigma_1 = 0$ on the Enceladus sections.

Table 4 Energies used in the construction of the surfaces of section and IPS, and the main regimes of motion in the corresponding sections

Figure	Energy level ($\times 10^{-12}$)	Regimes of motion
4	$l_1/-6.25$	RE, RDIP, RDI
6	$l_2/0.353588$	RE, RS1, RS2, RS3, RS4, RDI
9(a)	$l_3/1.71127$	RE, RS1, RS2, RS3, RS4, RDI
9(b)	$l_4/2.55203$	RE, RS1, RS2, RS3, RS4, RDI
9(c)	$l_5/4.46777$	RE, RS2, RS3, RS4, RDI
9(d)	$l_6/4.58145$	RE+RS2
10(a)	$l_7/6.84695$	RE, RS3, RS4, RDI
10(b)	$l_8/6.98703$	RS3, RS4, RDI
10(c)	$l_9/8.74751$	RE, RS4, RDI
10(d)	$l_{10}/9.72412$	High order secondary resonances, RE, RDI
10(e–f)	$l_{11}/10.55915$	RE, RDI

For each initial condition, the orbit is Fourier analyzed with a FFT, and the IPS are constructed showing, for each initial condition, the main frequencies present in the oscillation of the x_1 variable. Then, in the spectrum, we consider only peaks with amplitudes greater than a prefixed fraction (usually 0.1% of the largest peak in the spectrum). The spectrum of the solutions obtained with the two-degrees of freedom dynamical system given by Eq. (12) has two fundamental frequencies, their harmonics and linear combinations. In fact, each angular variable representing the variations of the satellites orbits, oscillates with two independent frequencies. We will call the independent frequencies associated to σ_1 and σ_2 by proper frequencies.

The study of the phase space of our system will be done in the next sections with some surfaces of sections and IPS, considering some convenient level curves of Fig. 2. The values of energy used in the surfaces of sections are given in Table 4.

4.1 The main resonances

Let us begin with the level curve l_1 in Fig. 2, where the value of the energy is $H = -6.25 \times 10^{-12}$. At this energy, three main structures appear, corresponding to the centers of the main regimes of motion.

Regime RDI. The fixed point indicated by RDI in Fig. 4(a) is the center of the true libration of σ_2 around π, while σ_1 and $\Delta\varpi = \sigma_1 - \sigma_2 = \varpi_1 - \varpi_2$ circulate in retrograde direction. The regime of motion RDI is associated to the Dione main resonance, which separatrix is indicated by SDI. In Fig. 5, in order to illustrate the details of the regimes of motion, we show the time-evolution of the angles of some orbits with initial conditions very near the centers of RDI and RE. In Fig. 5(a), we can see two periods in the time variation of σ_2: one associated to the proper motion of σ_1, with period of about 3 years, and the other associated to the proper libration of σ_2 itself, with period of about 30 years. From Fig. 4(b, c) we can see that the center of the regime RDI appears in the Enceladus section almost hidden and squeezed against the border of the figure, on the right. The separatrix SDI cannot be seen easily in the surface of section, but can be identified in the IPS shown in Fig. 4(d): near SDI, the distribution of the main frequencies are not smooth and their values tend to zero, characterizing chaotic motion. The main frequencies in the IPS are defined in the Appendix.

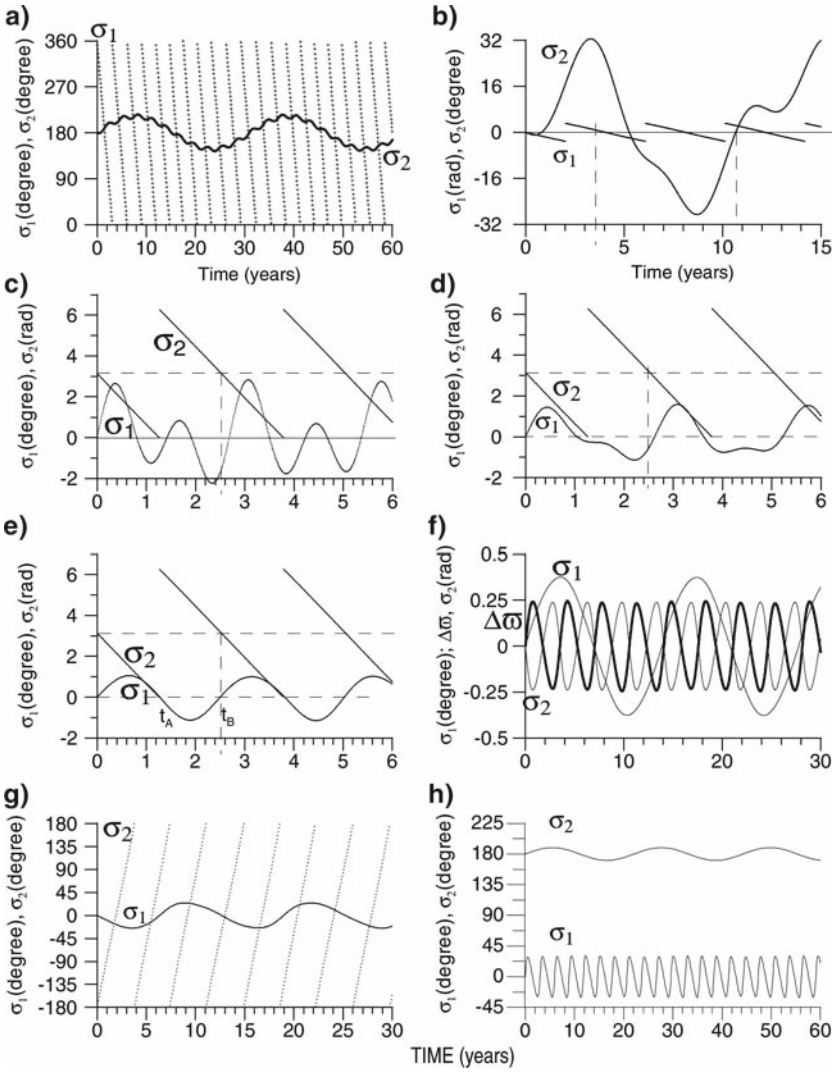

Fig. 5 Time variation of the critical angles around the centers of the main regimes of motion in different regions of the phase space. (**a**) Initial condition near the center of RDI shown in Fig. 4(a). (**b**) The same as (**a**) for RDIP. (**c**) Initial condition around the center of RE shown in Fig. 4(b), for $e_1 = 0.0005$. (**d**) The same as (**c**), for $e_1 = 0.0005115$. (**e**) The same as (c), for $e_1 = 0.000517$. (**f**) Initial condition around the center of RE in the case of Fig. 6. The bold line shows $\Delta\varpi$. (**g**) The same as (**f**), in the case of Fig. 9(a). (**h**) The same as (**f**), in the case of Fig. 10(e,f). In all figures, excepting (**a, g, h**), the scale of the *y*-axis must be read in degree or radian

Regime RDIP. The fixed point indicated by RDIP in Fig. 4(a) is the center of the libration of σ_2 around zero, where σ_1 circulates in retrograde direction (Fig. 5b). This motion of the critical angle σ_2 is of the type of a paradoxical libration (see Sect. 2.2). In the paradoxical libration, the forced center due to resonance exists, which is located very near the origin. This kind of motion is different from true libration associated to the separatrix SDI defining the main resonance zone around RDI.

Regime RE. The fixed point RE shown in Fig. 4(b) represents a periodic orbit with σ_1 librating about zero, and σ_2 and $\Delta\varpi$ circulating in retrograde and direct direction, respectively. In the sequence shown in Fig. 5(c–e), we see the time evolution of σ_1 and σ_2 for several initial conditions near the center of RE. The proper oscillations associated to the motion of σ_1 and σ_2 have periods of about 1.4 and 2.5 years, respectively. Figure 5(c) shows that, at a distance rather far from the center of RE, the amplitude of proper libration of σ_1 is large, and the presence of the second frequency associated to σ_2 is almost not visible. As we take initial conditions near the center RE, the amplitude of the proper motion of σ_1 becomes smaller, and the oscillation associated to the motion of σ_2 dominates (Fig. 5d). Very near the center of RE, the amplitude of proper libration of σ_1 tends to zero, and only the oscillations associated to σ_2 are visible in the motion of σ_1 (Fig. 5e).

It is interesting to discuss Fig. 5(e) in more detail. Note that even though the initial condition is very near the center of RE, where the amplitude of proper motion of σ_1 is almost zero, σ_1 remains oscillating about zero with the frequency of σ_2. This kind of motion can be understood geometrically as follows. Let us consider the three instants of time, indicated in Fig. 5(e) by $t = 0$, t_A and t_B. When $t = 0$, $\sigma_1 = 0$, $\sigma_2 = \pi$, $\Delta\varpi = -\pi$, which means that the orbits are initially anti-aligned. In t_A, $\sigma_1 = \sigma_2 = 0$ and therefore $\Delta\varpi = 0$, which means that now the orbits are aligned. In t_B, after one period, $\sigma_1 = 0$, $\sigma_2 = \pi$, and therefore the satellites orbits return to the initially anti-aligned configuration. That is, exactly at the center of RE, the motion of the pericenters of both orbits varies periodically between anti-aligned and aligned orbits, with the same period of σ_2.

Finally, we note that the motion of the critical angle σ_1 around RE center is of the kind of paradoxical libration, similar to the center RDIP discussed above for the case of Dione. In that case, there was a true separatrix associated to the Dione resonance. In the present case of RE, however, there is no separatrix associated to the "true" resonance of Enceladus.

Now let us consider the level curve l_2 in Fig. 2. The surface of section and the corresponding IPS are shown in Fig. 6. At this energy, the period of proper libration of σ_1 around RE is about 14 years (Fig. 5f), in opposition to the $\approx$1.4 years shown in Fig. 5(c, d). At this energy, σ_2 and $\Delta\varpi$ also librate, and the period is about 3.5 years. This occurs because the centers of RDPI and RE coincide, but this point will be better explained in Sect. 4.3 when the dynamical map will be presented. The numerical values of the frequencies associated to the proper motion of σ_1 and σ_2 around RE can also be seen in Fig. 6(c), which shows the individual power spectra (IPS). The main frequencies are indicated by f_{σ_1} and f_{σ_2}, and the other frequencies associated to harmonics are indicated by $2f_{\sigma_1}, 3f_{\sigma_1}$.

4.2 Secondary resonances

Inspection of all plots in Fig. 6 shows that, between the domains of the main regimes RE and RDI, there are several other small structures. In fact, in this portion of phase space the other centers are associated to exact commensurability between the proper frequencies of σ_1 and σ_2. We will refer to these centers as secondary resonances, which will be named by RS1, RS2, ... etc. In the similar way, the dynamics in the vicinity of the fixed points is very particular, so that we call regime RS1, RS2 etc, for each secondary resonances, respectively.

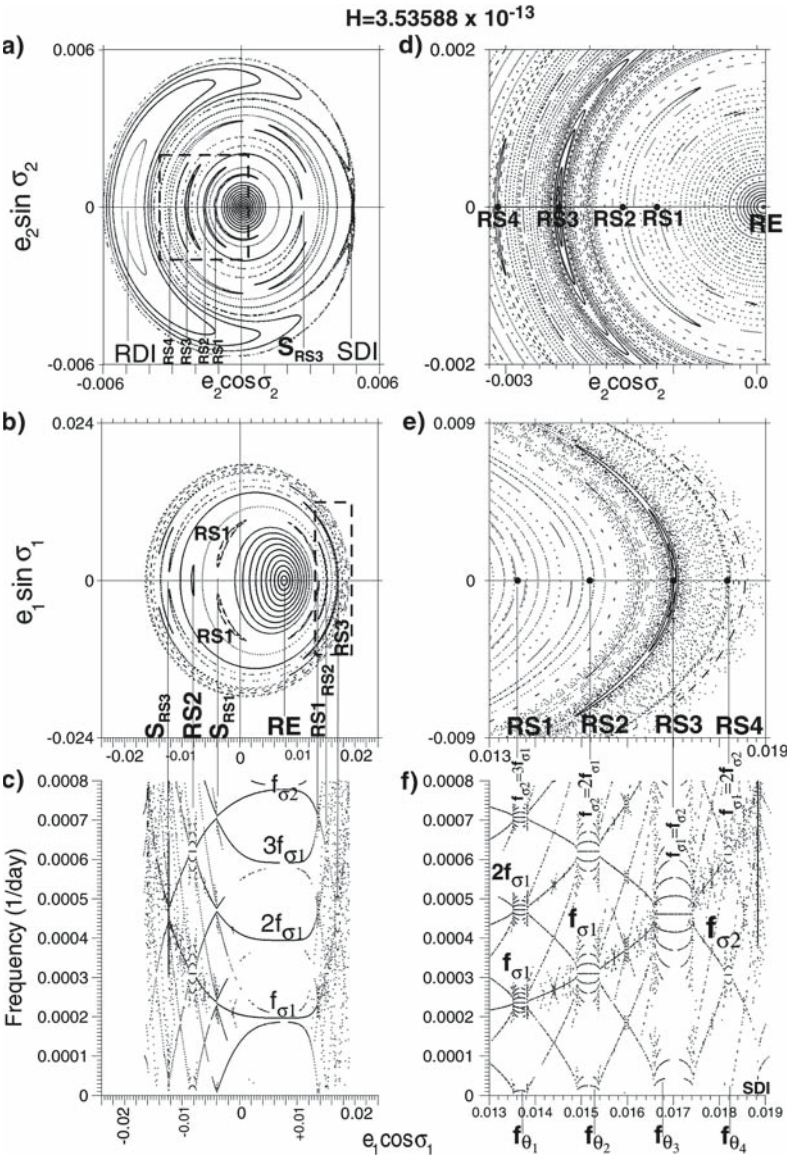

Fig. 6 (**a**) Dione section. (**b**) Enceladus section. The regimes of motion indicated by RE, RDI, RS1-RS4 are discussed in Sects. 4.1–4.2. (**c**) IPS corresponding to the interval of initial conditions used in (**a, b**). (**d, e**) Enlargements of the regions of phase space inside the dashed squares shown in (**a, b**), respectively. The black points near the centers of RS1, RS2, RS3 and RS4 have ordinates $e_1 = 0.013615, 0.01518, 0.017, 0.01817$, respectively, and correspond to initial conditions used in 7(**a**–**h**). (**f**) Details of a region at right of the IPS shown in (**c**)

Regime RS1. Fig. 6(b, e) show that the center RE is surrounded by three small islands. Figure 7(a) shows an orbit inside the domain of these islands: we can see that the evolutions of the critical angles are characterized by the retrograde circulation of σ_1 and direct circulation of σ_2. We note that inside the thin domain around this center,

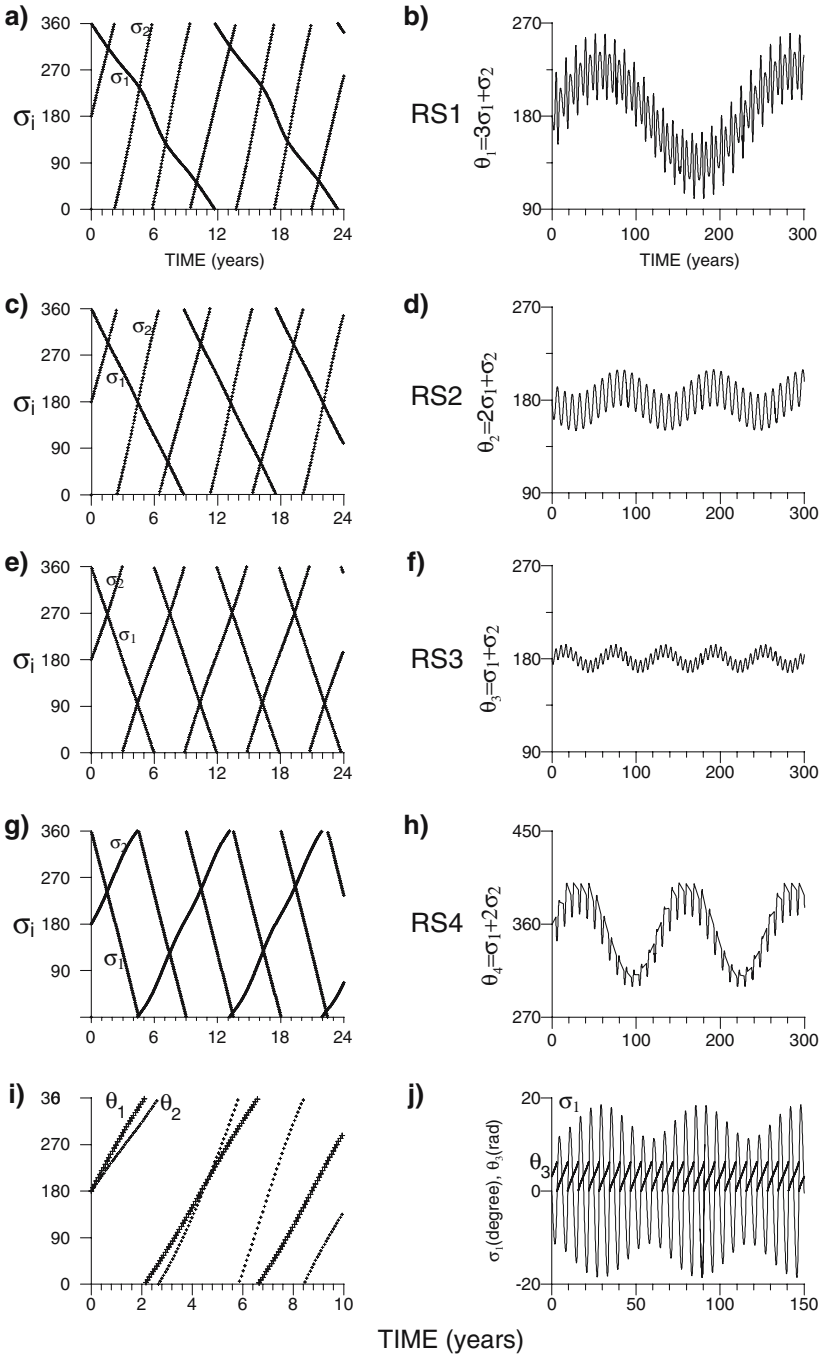

Fig. 7 (**a–h**). Left: Time evolution of the critical angles for the initial conditions indicated by black points shown in Fig. 6(**d, e**). Right: Corresponding time evolution of the variables θ_i associated to secondary resonances RS1–RS4. (**i**) Circulation of the variables θ_1 and θ_2 for initial condition around RS1 and RS2, respectively, in the cases shown in Figs. 9(a) (RS1) and 10(a) (RS2). (**j**) Libration of σ_1 and circulation of θ_3 for initial condition near the center of RS3 for $H = 7.40725 \times 10^{-12}$

denoted by RS1, the two fundamental frequencies have a ratio approximately equal to 3. In IPS given by Fig. 6(f) we can note that the loci of f_{σ_2} coincides with the loci of $3f_{\sigma_1}$ around RS1. In fact, well inside the center of RS1, we have $f_{\sigma_2} = 3f_{\sigma_1}$. Therefore, it is interesting to analyze the behavior of the variable $\theta_1 = 3\sigma_1 + \sigma_2$: Fig. 7(b) shows that θ_1 librates around π with period of 230 years. In Fig. 6(f), the line corresponding to this small frequency is indicated by f_{θ_1}.

The regime of motion RS1 is a clear example of a kind of motion which we will call by secondary resonance. In fact, dynamical system with two degrees of freedom is replete of secondary resonances between the main frequencies of the problem. The appearance of these secondary resonances depends on the region of phase space and the fixed parameters (Lichtenberg and Lieberman 1983; Lemaitre and Henrard 1990), and their importance in the dynamics of systems of satellites is discussed in several papers (Tittemore and Wisdom 1990; Malhotra and Dermott 1990; Champenois and Vienne 1999).

Regimes RS2, RS3, RS4. Figure 6 shows some additional secondary resonances associated to fixed points RS2, RS3, RS4. The angular variables associated are $\theta_2 = 2\sigma_1+\sigma_2, \theta_3 = \sigma_1+\sigma_2, \theta_4 = \sigma_1+2\sigma_2$, respectively. For the energy used in Fig. 6, around the fixed points of RS2, RS3 and RS4, the variables θ_2, θ_3 and θ_4 librate around π, π and zero, respectively (Figs. 7c–f). We have selected these three secondary resonances because they are associated to low order commensurabilities between σ_1 and σ_2.

We note two additional points: (1) The amplitude and period of libration of θ_i depend on the initial condition and the amplitude tends to zero around the fixed points. In this case, only the amplitudes associated to the proper modes of σ_1 and σ_2 can be seen in the time evolution of the orbits. (2) The domain of the centers are separated by chaotic separatrices. In Fig. 6(a, b), we indicate the separatrices associated to RS1, RS2 and RS3 by S_{RS1}, S_{RS2} and S_{RS3}, respectively.

4.3 Dynamical map

Now that we have discussed the main regimes of motion and the time variation of typical orbits of each regime, we are in position to investigate some qualitative features of the orbits. More precisely, with the use of the dynamical map we can get a general view of the distribution of chaotic and regular orbits in the (e_1, e_2) plane. It is based on the spectral number (Michtchenko and Ferraz-Mello 2001; Ferraz-Mello et al. 2005), and is constructed integrating the averaged equations of motion for initial conditions in a fine grid of 801×301 points in the representative plane shown in Fig. 8. For each integration, the solutions are Fourier analyzed. The spectral number N is defined as the number of significant spectral peaks with amplitude greater than a cut limit, for instance, 0.1% of the highest peak of the variable x_1. Therefore each point of the grid is labeled with this N and the grid is plotted in a gray code map.

The white strips in Fig. 8 correspond to the immediate neighborhood of periodic orbits, where only one significant peak is seen in the spectrum ($N = 1$). The light regions (small N) correspond to regular (periodic or quasi-periodic) orbits, while darker regions (large N) indicate nonharmonic or chaotic motion associated to the separatrices of the problem. As mentioned before all the initial conditions to generate the surfaces of section are extracted from the representative plane. Therefore the general features of the dynamics revealed by sections (mainly related to fixed points) can be identified on the representative plane. In Fig. 8 some level curves of Fig. 2 are

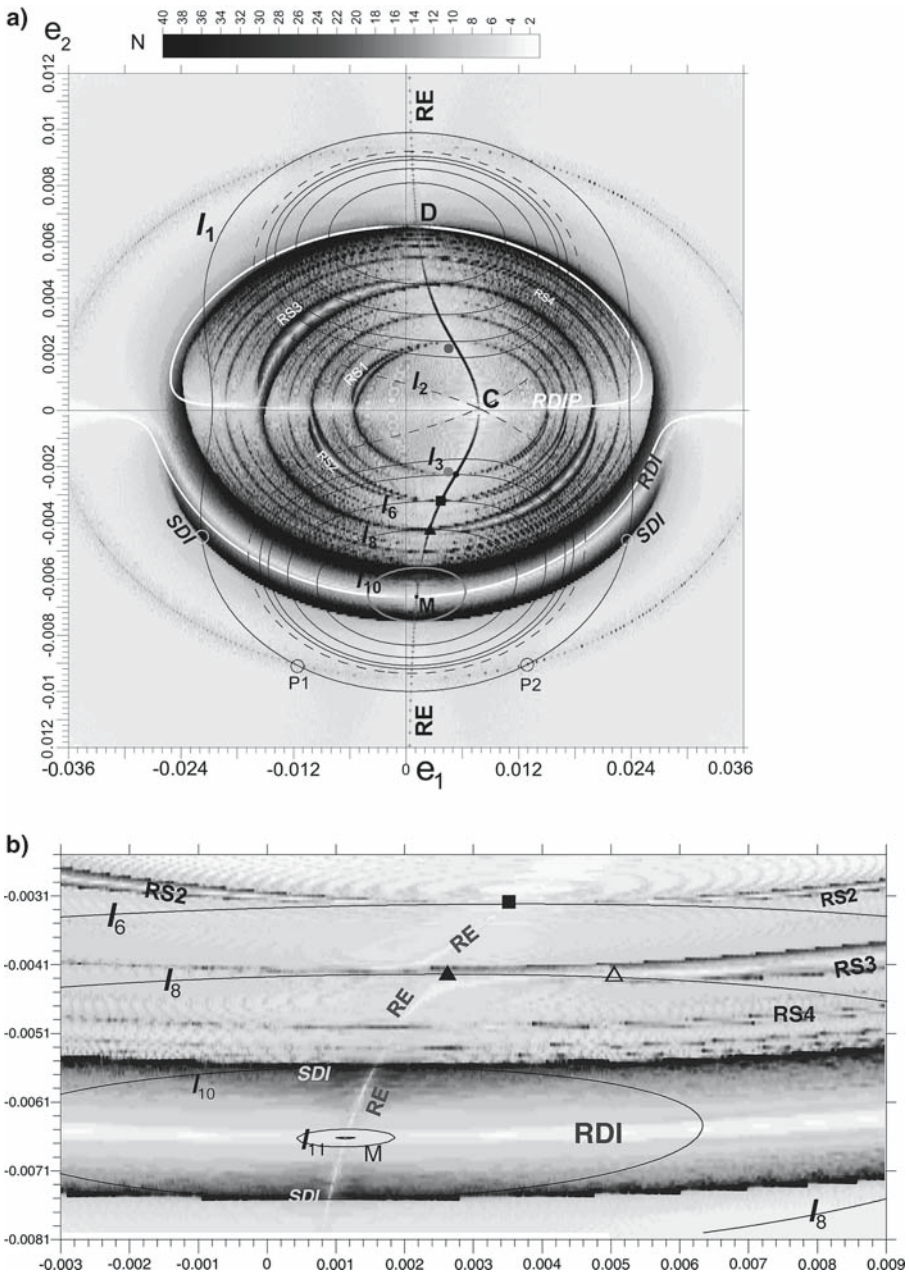

Fig. 8 (**a**) The dynamical map of the 2/1 Mean–Motion resonance for E–D system. N is the spectral number defined in Sect. 4.3 All labels RDI, RE, RS1–RS4 etc are defined in Sects. 4.1 and 4.2. The scales of the axes are not the same for better resolution. Some level curves shown in Fig. 2 are also plotted. The black and white bold lines are the loci where $\dot{\sigma_1} = 0$ and $\dot{\sigma_2} = 0$, respectively. The black symbols (point, square, triangle) show the positions where RE touches the centers of RS1, RS2 and RS3, respectively. The gray points near RE represents the actual possible position of the pair E–D in the plane. Open circles indicate intersection with l_1. (**b**) Detail of (**a**) around the point of maximum energy M. The open triangle gives the position of the center of RS3 on the level curve l_8

also shown superimposed to the dynamical map. With this technique, the fixed points like RDI, RDIP, RE, RS1 etc can be identified on the corresponding level curves.

The letters RE, RDI, RDIP in Fig. 8 are fixed points corresponding to the centers of the islands obtained in Figs. 4 and 6. Since they represent stable orbits, usually the motion is regular in a small vicinity of these periodic orbits. In the particular case of RE, RDI and RDIP, the path of their periodic orbits can be obtained analytically in the plane (e_1, e_2), through Hamilton equations $\mathrm{d}\sigma_1/\mathrm{d}t = \partial H/\partial I_1 = 0$ and $\mathrm{d}\sigma_2/\mathrm{d}t = \partial H/\partial I_2 = 0$. The loci of RE is obtained directly from $\mathrm{d}\sigma_1/\mathrm{d}t = 0$ and is indicated in Fig. 8(a) by black bold line, while the loci of RDI and RDIP come from $\mathrm{d}\sigma_2/\mathrm{d}t = 0$ and are indicated by white bold lines. These curves intercept themselves in the zero-gradient points D, C and M and there is a good agreement between the analytical results and those obtained with the map. Note that at the point C, the regimes RE and RDIP coincide. We can consider the level curve l_2 a bifurcation value which probably may give rise to different periodic orbits associated to secondary resonances.

Figure 8(a) shows two gray points drawn in the regions defined by $\sigma_1 = 0$, $\sigma_2 = 0$ and $\sigma_1 = 0$, $\sigma_2 = \pi$, where we have used the values of the eccentricities given in Table 1. These points can be considered as projections representing the approximated positions of the actual pair E–D in the representative plane of initial conditions. In fact, according to Sect. 2.2, the current configuration system is near RE since σ_1 librates about zero, and the white points are very near the white strips associated to RE. Moreover, according to Sect. 2.2, actually σ_2 circulates in direct direction, what might occur along both families of initial conditions, r_2 and r_3, as we will see below in Sect. 4.4.

The intersections of the energy levels l_1 and l_2 with the white and black strips associated to all centers and separatrices in Fig. 8 occur for values of e_1 and e_2 which are in good agreement with Figs. 4 and 6. For instance, the white circles on l_1 indicated the loci of the separatrix SDI between regimes RE and RDI. This separatrix is associated to Dione resonance, not to paradoxical libration of Enceladus RE. In the same way, the intersection of the outer "black ring" and l_1 indicated by black circles denoted by P1 and P2 corresponds to separatrices associated to very high order secondary resonances, as will be discussed in the Appendix.

4.4 Continuation of the regimes of motion

In order to follow the evolution of the centers of the main regimes and secondary resonances for larger values of energy, let us consider the level curves l_3–l_{11} in Fig. 2. Figure 9 shows, in each plot (a–d), the Enceladus sections (top) and IPS (bottom). At energies used in Fig. 9, the main quantitative changes are related to regimes RE and RS1, and let us discuss only these two cases. In the case of RE, σ_2 now circulates in direct direction (Fig. 5g), because we are in the inner family r_2 (the direction of circulation of σ_2 depends on the set of initial condition: direct and retrograde circulation in the inner and outer families, respectively). Comparing all IPS shown in Figs. 9 and 6(c), we can see that the values of the fundamental periods of σ_1 around RE did not change significantly in this portion of the phase space (compare also Fig. 5(f,g) and IPS). In the case of RS1, we can see from Fig. 9(a) that the center of the islands are located on the right of the figure, and therefore the proper motion associated to σ_1 is the libration about zero. In this case, inside RS1, the variable $\theta_1 = 3\sigma_1 + \sigma_2$ now circulates (Fig. 7i) because σ_1 librates while σ_2 circulates. Note that σ_1 begins to librate in RS1 because its domain becomes smaller than that observed in Fig. 6(b), even the

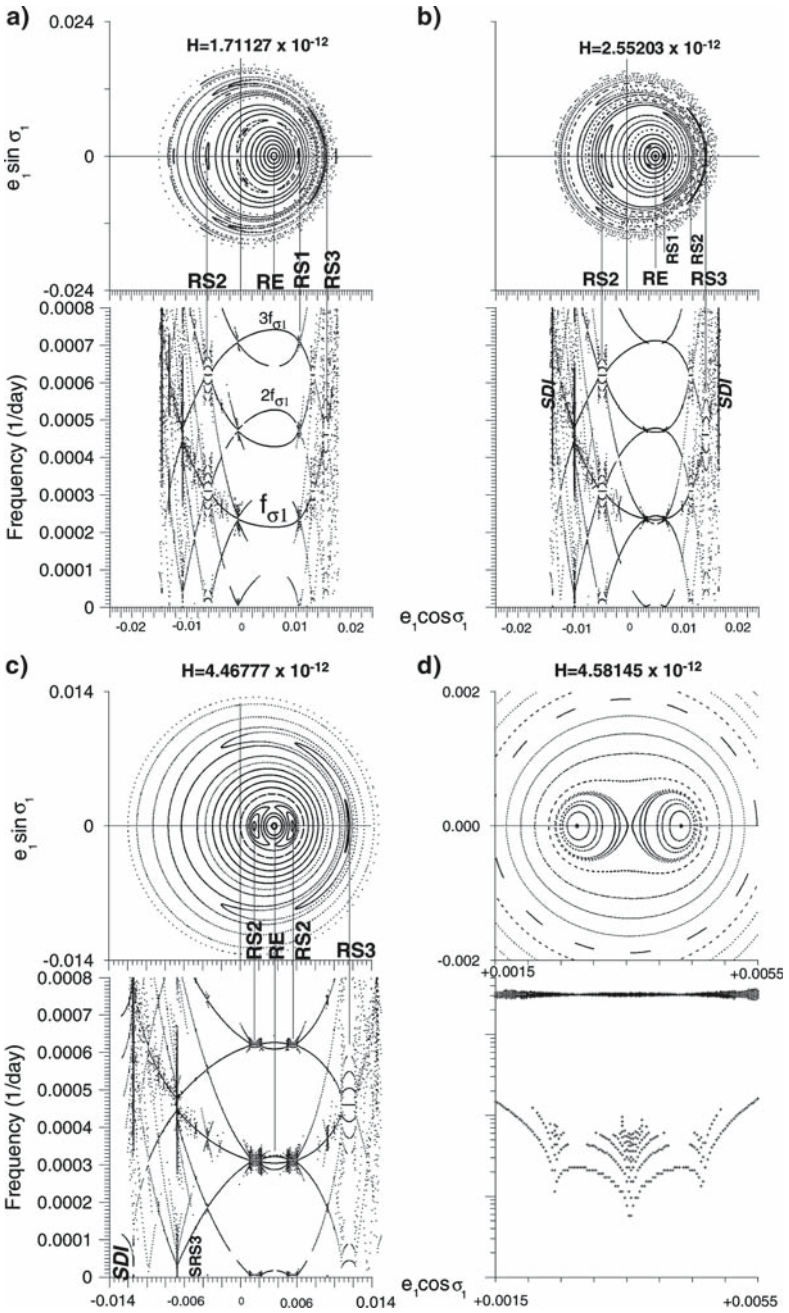

Fig. 9 (**a–d**) Enceladus section (top) and IPS (bottom), for different values of energy. The value of energy is shown at the top of Enceladus sections. The regimes of motion are indicated at the bottom. (**a**) Energy level l_3. (**b**) Energy level l_4. The vertical "bars" near the separatrix SDI is indicated in the IPS. (**c**) Energy level l_5. (**d**) Energy level l_6

forced eccentricity of RE is smaller. (In fact, for energies larger than l_1, the value of the forced eccentricity of the center of RE decreases, as we can see from the loci of RE given in Fig. 8.)

For energy given in Fig. 9(b), we see that the domain of RS1 becomes smaller. In fact, for slightly larger values, the islands around the fixed point RS1 vanish. In Fig. 8(a), the black point located between l_3 and l_6 on the energy level $H = 2.63604 \times 10^{-12}$, shows the position on the representative plane where the periodic orbits associated to RS1 and RE cross themselves. It is interesting to note that the gray points associated to the actual position of the pair E–D in the representative plane are also located between l_3 and $H = 2.63604 \times 10^{-12}$. This suggests that the current configuration of the pair E–D is near the loci of a secondary resonance of the kind of RS1. It is worth to notice that in this work we do not intend to give the precise location of the system in the representative plane (see discussions in Sects. 2.2 and 3).

Increasing the energy, the center of RE appears isolated again on the surface of section and on the IPS, as shows Fig. 9(c). The main changes are related to the domain of RS2, which becomes smaller in Enceladus section. Figure 9(c) shows that RS2 is located on the positive part of x-axis, and therefore σ_1 librates about zero for all initial conditions within RS2. In this case the variable θ_2 no more librates (Fig. 7i). The distribution of frequencies of the higher harmonics in the IPS also suffers changes. For instance, the "long-period" oscillation, occurs due to a quasi-commensurability between the proper period of libration of σ_1 and the period of circulation of σ_2 in the 2/1 ratio. Very near the center of RE, the amplitude of these harmonics tends to zero; but, sometimes, this is not visible mainly when the cut limit adopted is very low (see for instance Fig. 10b below).

For larger values of energy $H = 4.58145 \times 10^{-12}$ (l_6), the islands around RS2 vanish. Figure 9(d) shows the Enceladus section and IPS around RE where the fixed points RE and RS2 are very near. In the dynamical maps shown in Fig. 8(a,b), the position of the encounter between RE and RS2 is indicated by a black square.

Figure 10(a) shows that at energies given approximately by $H = 6.84695 \times 10^{-12}$ (level curve l_7), the domain of RE in the surface section is small and slightly smaller than the domain of RS3 (the forced eccentricity of RE is very small). Note that although the curves in the surface of section may suggest libration of σ_1 within the banana separatrix of RS3, both critical angles remain circulating, similar to the case shown in Fig. 7(e). Figure 10(b) shows the presence of only one fixed point (RS3), what means that at these energies the periodic orbit associated to RE suffers another encounter with low order secondary resonances (the two others cases discussed here, appeared when RE encountered RS1 and RS2). To better understand the absence of RE in Fig. 10(b), consider Fig. 8: the level curve l_8 crosses the separatrix of RS3 in the point indicated by a black triangle, and touches only the periodic orbit associated to RS3 at right, indicated by an open triangle. The IPS shown in Fig. 10(b) shows a complex distribution of harmonics around the lines associated to f_{σ_1} and f_{θ_3}, leading to σ_1 and θ_3 alternate their motion between libration and circulation except for initial condition very near the fixed point of RS3. Increasing the energy, σ_1 librates around zero for trajectories near the fixed point of RS3 while σ_2 and θ_3 circulate, similar to the case of RE studied before (see Fig. 7j). We can therefore denote this new regime of motion by RE again.

The above scenario, characterized by repeated encounters between the fixed points associated to RE and secondary resonances, occurs until energies $H \approx 9.72412 \times 10^{-12}$, which corresponds to the value of the level curve l_{10}. For instance, Fig. 10(c) shows the

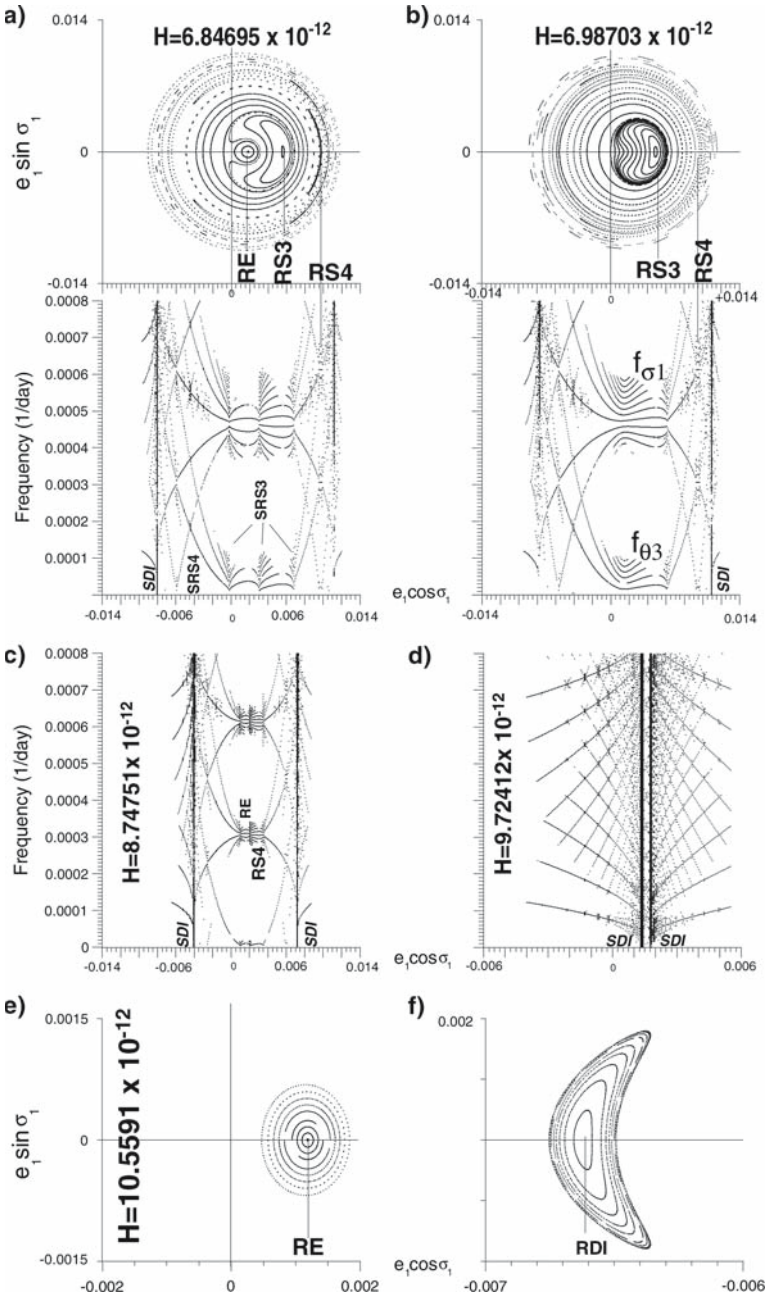

Fig. 10 (**a**,**b**) The same as Fig. 9. Since the domain of Enceladus section and IPS are small, we have changed the scale of the figures for better resolution. (**a**) Energy level l_7. The separatrices SRS3 and SRS4 are indicated in the IPS. (**b**) Energy level l_8. f_{σ_1} and f_{θ_3} indicate the curves in the IPS associated to proper frequencies of σ_1 and θ_3, respectively. (**c**) IPS for the energy level l_9. (**d**) IPS for the energy level l_{10}. (**e**) Enceladus section for the energy level l_{11}. (**f**) Dione section corresponding to (**e**)

IPS constructed for the value of energy where the encounter between RE and RS4 occurs. Figure 10(d) shows the IPS corresponding to level curve l_{10}. On this energy level, almost all initial conditions belonging to inner family r_2 are located very close the domain of SDI, explaining the complex structure seen in Fig. 10(d) around a small center corresponding to RE.

The energy level l_{10} defines the region of initial conditions denoted by Region D in Sect. 3. Fig. 10(e, f) shows Enceladus and Dione sections, respectively, corresponding to energy level l_{11} well inside Region D. At these values of energy, the dynamics is very regular, with the predominance of the two centers associated to RE and RDI. Fig. 10(e, f) shows that in the Enceladus section, RE is the dominant regime of motion, whereas in the Dione section RDI dominates the phase space. We can see that the domain of RE and RDI are very small, and σ_1 and σ_2 librates about zero and π, respectively, for all trajectories (see Fig. 5g). The Region D corresponds to the co-rotation zone (e.g. Michtchenko et al. 2006). The periodic orbits associated to the two main resonances inside Region D are also seen in Fig. 8(b).

The small domains of the regimes in the sections occur since for these energies the system is near the point of the maximum ($H \approx 10.5745 \times 10^{-12}$), and beyond this value the quartic Hamiltonian has no real roots and no motion is possible.

5 Conclusions and discussion

The main objective of this paper is to present a general study of the dynamics of a pair of satellites similar to Enceladus and Dione with a planar model with two degrees of freedom. Using the surfaces of section and spectral analysis techniques conveniently designed for the present Hamiltonian, we studied in details a particular region of the phase space inside the 2/1 resonance and assigning for the constants and parameters the current values of the E–D pair. The approximate position of the system in the representative plane of initial conditions confirm the known fact that, for low eccentricities, the two resonances, the Enceladus (RE) and Dione (RDI), are well separated, due to high value of Saturn oblateness. We found also that the phase space is filled with several secondary resonances. Then we studied in detail four of them (RS1, RS2, RS3, RS4). The current position of Enceladus is probably near one secondary resonance of the kind of RS1.

The complexity of the 2/1 resonance for Uranus' regular satellites was already pointed by Tittemore and Wisdom (1990). In their case, the small oblateness of Uranus can cause the overlap of the main resonances, which enhances the difficulties of the problem. In our case, the resonances are well separated, however the phase space is replete of numerous secondary resonances. In the literature (see Peale 1986, and references therein), there are several studies about the dynamics of the pair E–D with integrable models. Our results show that the presence of several secondary resonances of low order near to the main resonances makes the 2/1 resonance much more complex. Therefore, systems of satellites like Enceladus and Dione where the parent body have large oblateness must be dealt with models more general than those reducible to one degree of freedom.

Secondary resonances might have played important role in the past, although currently, they do not cause any significant chaos. The role of secondary resonances during the tidal evolution of natural satellites was subject of several works (e.g.,

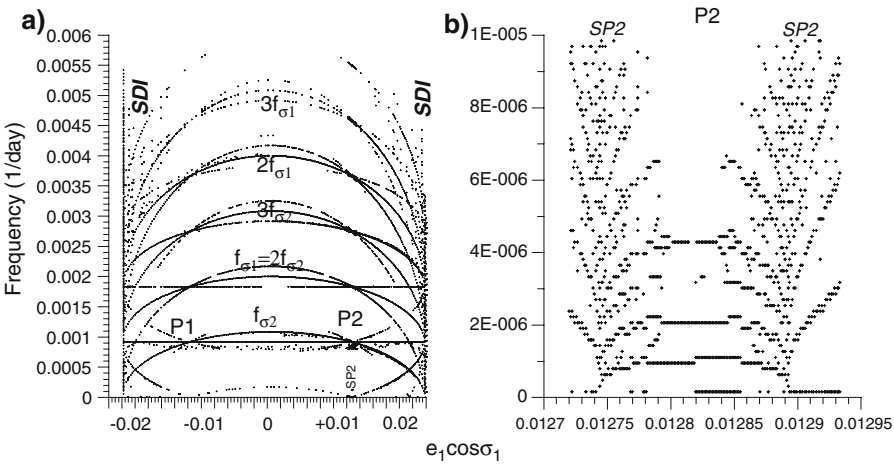

Fig. 11 (**a**) Individual dynamical map corresponding to Fig. 4(b). P1, P2 are also shown in Fig. 8(a) by black circles. (**b**) Details of the initial conditions around P2 shown in (**a**)

Tittemore and Wisdom 1990; Champenois and Vienne 1999; and references therein). In our case, a similar investigation will be presented in a future work.

Acknowledgements This work has been supported by Fapesp (Proc. 04/11826-8, 04/15787-7). The authors thank the referees A. Lemaitre and K. Tsiganis for their valuable suggestions and comments. R. A. Jacobson is gratefully acknowledged for sending us some recent data for Saturn system, and O. C. Winter for some discussion. T. Yokoyama thanks CNPQ and FUNDUNESP for partial financial support.

Appendix

This Appendix shows the IPS corresponding to some initial conditions related to Fig. 4(b–d). In this case the motions are very regular (except near the separatrices), and, in order to identify the main frequencies and their harmonics—which are indicated in Fig. 11(a)—we used the cut amplitude equal 0.01% of the largest pick. The smaller frequency is associated to high order secondary resonances, whose value tends to zero around the separatrices denoted by SP2 and involves the region P2—shown in detail in Fig. 11(b). In Fig. 11(b) the cut amplitude is 0.001% of the main peak. Note that P2 is the small portion of the "black ring" seen in Fig. 8(a). The dynamics along the very small domain inside P2 do not show new features, and the two critical angles circulate in retrograde direction.

References

Beaugé, C., Callegari Jr., N., Ferraz-Mello, S., Michtchenko, T.A.: Resonances and stability of extrasolar planetary systems. In: Knežević, Z., Milani A. (eds.). IAU Colloq. **197**, 3–18 (2005)

Bevilacqua, J.S., Sessin, W.: First order perturbation in the Enceladus–Dione system. Rev. Mex. Astr. Astrof. **14**, 627–630 (1987)

Bevilacqua, J.S., Sessin, W., Chen, J.: Periodic orbits in the Enceladus–Dione system. In: Vieira Martins, R. et al. (eds.) Orbital Dynamics of Natural and Artificial Objects, pp. 13–21. Observatório

Nacional, Rio de Janeiro, Brasil (1989)
Callegari, Jr. N., Michtchenko, T.A., Ferraz-Mello, S.: Dynamics of two planets in the 2/1 mean–motion resonance. Celest. Mech. Dyn. Astr. **89**, 201–234 (2004)
Callegari, Jr. N., Ferraz-Mello, S., Michtchenko, T.A.: Dynamics of two planets in the 3/2 mean-motion resonance: application to the planetary system of the pulsar PSR B1252+12. Celest. Mech. Dyn. Astr. **94**, 381–397 (2006)
Champenois, S., Vienne, A.: Chaos and secondary resonances in the Mimas-Tethys system. Celest. Mech. Dyn. Astr. **74**, 111–146 (1999)
Ferraz-Mello, S: First-order resonances in satellites orbits. In: Ferraz-Mello, S., Sessin, W. (eds.) Resonances in the Motion of the Planets, Satellites and Asteroids, pp. 37–52. IAG/USP, Sao Paulo (1985)
Ferraz-Mello, S., Dvorak, R.: Chaos and secular variations of planar orbits in 2:1 resonance with Dione. Astr. and Astrophys. **179**, 304–310 (1987)
Ferraz-Mello, S., Michtchenko, T.A., Beaugé, C.: Regular motions in extra-solar planetary systems. In Steves, B.A., Maciejewicz, A.J., Hendry M. (eds.) Chaotic Worlds: From Order to Disorder in Gravitational N-Body Systems, pp. 255–288. Springer, Dordrecht. ArXiv: astro-ph/0402335 (2006)
Ferraz-Mello, S., Michtchenko, T.A., Beaugé, C., Callegari Jr. N.: Extra-solar planetary systems. In: Dvorak, R. et al. (eds.) Lecture Notes in Physics, **683**, 219–271 (2005)
Goldreich, P.: An explanation of the frequent occurence of commensurable mean motion in the solar system. MNRAS **130**, 159–181 (1965)
Henrard, J., Lemaitre, A.: A second fundamental model for resonance. Celest. Mech. **39**, 197–218 (1983)
Hori, G: Mutual perturbations of 1:1 commensurable small bodies with the use of canonical relative coordinates. Part I. In: Ferraz-Mello, S., Sessin, W. (eds.) Resonances in the Motion of the Planets, Satellites and Asteroids., pp. 33–66. IAG/USP, Sao Paulo (1985)
Jacobson, R.A.: The orbits of the major Saturn Satellites and the gravity field of Saturn from spacecraft and Earth-based observations. Astron. J. **128**, 492–501 (2004)
Jacobson, R.A., Antreasian, P.G., Bordi, J.J., Criddle, K.E., Ionasescu, R., Jones, J.B., Mackenzie, R.A., Pelletier, F.J., Owen, W.M., Roth, D.C., Stauch, J.R.: The gravity field of the Saturnian system and the orbits of the major Saturnian satellites. Bull. Am. Astron. Soc. **37**, 729 (2005)
Jacobson, R.A., Antreasian, P.G., Bordi, J.J., Criddle, K.E., Ionasescu, R., Jones, J.B., Mackenzie, R.A., Meek, M.C., Parcher, P., Pelletier, F.J., Owen, W.M., Roth, D.C., Roundhill, I.M., Stauch, J.R.: The gravity field of the Saturnian system from satellite observations and spacecraft tracking data. Astron. J. **132**, 2520–2526 (2006)
Jancart, S., Lemaitre, A., Istace, A.: Second fundamental model of resonance with asymmetric equilibria. Celest. Mech. Dyn. Astr. **84**, 197–221 (2002)
Karch, M., Dvorak, R.: New results on the possible chaotic motion of Enceladus. Celest. Mech. Dyn. Astr. **43**, 361–369 (1988)
Laskar, J., Robutel, P.: Stability of the planetary three-body problem I: expansion of the planetary Hamiltonian. Celest. Mech. Dyn. Astr. **62**, 193–217 (1995)
Lemaitre, A., Henrard, J.: On the origin of chaotic behavior in the 2/1 Kirkwood gap. Icarus **83**, 391–409 (1990)
Lichtenberg, A.J., Lieberman, M.A.: Regular and stochastic motion. Springer-Verlag, Heidelberg (1983)
Malhotra, R., Dermott, S.F.: The role of secondary resonances in the orbital history of miranda. Icarus **85**, 444–480 (1990)
Message, P.J.: Orbits of Saturn's satellites: some aspects of commensurabilities and periodic orbits. In: Steves, B.A., Roy, A.E. (eds.) The Dynamics of Small Bodies in the Solar System. Kluwer Academic Publishers, pp. 207–225 (1999)
Michtchenko, T.A., Ferraz-Mello, S.: Modeling the 5:2 mean–motion resonance in the Jupiter–Saturn planetary system. Icarus **149**, 357–374 (2001)
Michtchenko, T.A., Beaugé, C., Ferraz-Mello, S.: Stationary orbits in resonant extrasolar planetary systems. Celest. Mech. Dyn. Astr. **94**, 411–432 (2006)
Peale, S.J: Orbital resonances, unsual configurations and exotic rotation states among planetary satellites. In: Burns, J.A. (ed.) Satellites pp. 159–223 (1986)
Peale, S.J: Origin and evolution of the natural atellites. Ann. Rev. Astron. Astrophys. **37**, 533–602 (1999)
Peale, S.J: Tidally induced volcanism. Celest. Mech. Dyn. Astr. **87**, 129–155 (2003)

Spencer, J.R., Pearl, J.C., Segura, M., Flasar, F.M., Mamoutkine, A., Romani, P., Buratti, B.J., Hendrix, A.R., Spilker, L.J., Lopes, R.M.C.: Cassini encounters enceladus: background and the discovery of a south polar hot spot. Science **311**, 1401–1405 (2006)

Salgado, T.M.V., Sessin, W.: The 2:1 commensurability in Enceladus–Dione system. In: Ferraz-Mello, S., Sessin, W. (eds.) Resonances in the Motion of the Planets, Satellites and Asteroids, pp. 93–105. IAG/USP, Sao Paulo (1985)

Sessin, W., Ferraz-Mello, S.: Motion of two planets with periods commensurable in the ratio 2:1. Solutions of the Hori Auxiliaty System. Celest. Mech. **32**, 307–332 (1984)

Sinclair, A.T.: On the origin of the commensurabilities amongst the satellites of Saturn. MNRAS **160**, 169–187 (1972)

Sinclair, A.T.: A re-consideration of the evolution hyphotesis of the origin of the resonances among Saturn's satellites. In: Dynamical trapping and evolution in solar system; Proceedings of Seventy-four Colloquium, Gerakini, Greece, August 30-September 2, 1982 (A84-34976 16-89), Dordrecht, D. Reidel Publishing. Co., pp. 19–25 (1983)

Shinkin, V.N.: Approximate analytic solutions of the averaged three-body problem at first-order resonance with large oblateness of the central planet. Celest. Mech. Dyn. Astr. **79**, 15–27 (2001)

Tittemore, W., Wisdom, J.: Tidal evolution of the Uranian satellites I. Passage of Ariel and Umbriel through the 5:3 Mean-Motion Commensurability. Icarus **74**, 172–230 (1988)

Tittemore, W., Wisdom, J.: Tidal evolution of the Uranian satellites III. Evolution through the Miranda-Umbriel 3:1, Miranda-Ariel 5:3, and Ariel-Umbriel 2:1 Mean–Motion Commensurability. Icarus **85**, 394–443 (1990)